Received: 3 April 2017 | Accepted: 23 June 2017

DOI: 10.1002/er.3824

TECHNICAL NOTE

WILEY INTERNATIONAL JOURNAL OF ENERGY RESEARCH

Using high-HFP-content cathode binder for mitigation of heat generation of lithium-ion battery

Anh V. Le[1] | Meng Wang[1] | Daniel J. Noelle[2] | Yang Shi[2] | Y. Shirley Meng[3] | Dengguo Wu[4] | Jiang Fan[4] | Yu Qiao[1,2]

[1] Department of Structural Engineering, University of California, San Diego, La Jolla, CA 92093-0085, USA

[2] Program of Materials Science and Engineering, University of California, San Diego, La Jolla, CA 92093, USA

[3] Department of Nanoengineering, University of California, San Diego, La Jolla, CA 92093, USA

[4] American Lithium Energy Corporation, 1485 Poinsettia Ave #118, Vista, CA 92081, USA

Correspondence
Yu Qiao, Department of Structural Engineering, University of California, San Diego, La Jolla, CA 92093-0085, USA.
Email: yqiao@ucsd.edu

Funding information
Advanced Research Projects Agency - Energy, Grant/Award Number: DE-AR0000396

Summary

We investigate the effects of thermally sensitive binder (TSB) on the temperature increase of lithium-ion battery (LIB) coin cell subjected to severe mechanical abuse. The TSB is poly(vinylidenefluoride-*co*-hexafluoropropylene) (PVDF-HFP), similar to conventional poly(vinylidenefluoride) (PVDF) binder but with a significant hexafluoropropylene (HFP) content. The testing data show that by using TSB, the peak temperature increase of nail-penetrated LIB coin cell can be reduced by 20% to 40%, attributed to the softening of TSB that begins from ~80°C. The cycling performance of the LIB cells is also characterized. This research sheds light on the development of thermal-runaway mitigation techniques.

KEYWORDS

binder, electrode, lithium-ion battery, PVDF-HFP, thermal runaway

1 | INTRODUCTION

Developing advanced lithium-ion battery (LIB) is critical to many engineering applications, such as large-scale energy storage systems of smart grids and long-range electric vehicles (EV).[1,2] Among many energy storage techniques, including fuel cells,[3] flow batteries,[4] zinc-air (Zn-air) batteries,[5] lithium-sulfur (Li-S) batteries,[6] and supercapacitors,[7] LIB is most widely applied, thanks to its high energy density, relatively long cycle life, and relatively low cost per kW·h.[8] A LIB cell contains a positive electrode and a negative electrode, with an electrolyte-hosting membrane separator in between. The positive electrode, ie, the cathode, usually consists of lithium metal oxides as the active material (AM), carbon black (CB) as the conductive additive, and a polymeric binder, casted on an aluminum (Al) current collector. The negative electrode, ie, the anode, is often made of graphite and CB, casted on a copper (Cu) current collector.[9]

Usually, poly(vinylidene-fluoride) (PVDF) is used as the binder for the cathode, due to its excellent adhesion strength, compatibility with the high-voltage electrochemical reactions, and high processability with solvents and AM. In a few special cases, eg, plastic lithium ion batteries, poly(vinylidene fluoride-*co*-hexafluoropropylene) (PVDF-HFP) is favored as a hosting material for the electrolyte, because it absorbs more electrolyte than PVDF and, thus, increases the ionic conductivity. Compared to PVDF, PVDF-HFP contains a larger amount of amorphous phase; its strength and thermal stability are lower, especially in the presence of electrolyte. Consequently, the polymer binder in a regular LIB has a low HFP content and may be treated to enhance the

binding strength.[10] The use of PVDF-HFP in LIB is limited to membrane separators or for polymer electrolytes.

Recently, increasing attention is given to the robustness of battery system. Under normal working condition of LIB, the membrane separator prevents direct contact between the cathode and the anode.[11] Yet, such a structure is damage intolerant. If a LIB cell is subjected to mechanical abuse, the separator may be broken apart and result in internal shorting.

Because of their high ionic conductivity, flammable organic solvents are employed for the electrolytes in most of today's LIB systems. They cause major concerns regarding fire safety. In damaged high-energy cells, the local temperature can quickly reach over 300°C, accompanied by decomposition of AM and electrolyte with gaseous products, leading to fire or even explosion.[12] Previous arts on thermal-runaway mitigation include thermal fuses, positive thermal coefficient (PTC) devices, shutdown separators and additives, etc.[12] For instance, PVDF-HFP was used to construct low-melting-point membranes, which can close the pores as the local temperature reaches the set point.[13] However, under severe mechanical abuses, rupture of the membrane separators is inevitable. More efficient approaches should be employed to increase the internal impedance around the damaged electrode areas.

In the past few decades, a few studies have focused on developing thermally responsive electrodes by adding positive temperature coefficient (PTC) materials. As local temperature reaches ~140°C, phase transition of the PTC material happens, and it expands significantly, cutting off the ion/electron transportation paths near the internally shorted sites and, therefore, reducing the heat generation rate.[14,15] One issue of this technique is that, with the PTC additives, the manufacturing procedure of LIB may be adjusted.

In this paper, we demonstrate that, instead of using PTC additives, the binder of LIB electrode can be thermally sensitive, by using PVDF-HFP. This technique requires no major variation in conventional slurry processing or increase in cell mass; ie, the specific energy of the battery remains the same. The thermally sensitive binder (TSB) would fail at ~110°C, disintegrating the electrode components. As the internal impedance rises, the heat generation is considerably slowed down. Such a technique has important relevance to LIB cells and packs where the system robustness is of a high priority and the fire hazard must be minimized.

2 | EXPERIMENTAL

For the positive electrode, $LiNi_{0.5}Mn_{0.3}Co_{0.2}O_2$ (NCM-04ST from TODA America), which will be referred to as NMC532 in the following discussion, was chosen as the AM. The average particle size of NMC532 was 10 μm to 20 μm. Poly(vinylidene-fluoride) (PVDF), with the molecular weight, M_w, of 180 000 (Arkema, Kynar® 711) was chosen as the reference binder. We tested a set of TSB of PVDF-HFP, with various HFP contents, as summarized in Table 1. The conductive additive was CB nanoparticles (CNERGY-C65 from TIMCΛL). The weight ratio among AM, binder, and CB was 93:4:3, typical for LIB coin cells.

For the negative electrode, the AM was artificial graphite (AG) (MTI Corp, product code EQ-Lib-CMSG). The binder was a blend of carboxymethyl cellulose (CMC) and styrene butadiene rubber (SBR), with the CMC-to-SBR mass ratio of 2:2. The binder content in anode was 4 wt% of all solid components. The SBR was obtained from MTI (Product Code EQ-Lib-SBR). The CMC sodium salt (CMC-Na) was obtained from Sigma-Aldrich (Product Code 1001817659). The CMC-SBR binder has been commonly used in anodes of commercial LIB cells. We also tested PVDF as the binder in anode, which is commonly used in laboratory testing. The PVDF binder for anode was Kynar® HSV 900, obtained from Arkema. Its degree of polymerization was above 500 000, and the binder content was 6 wt% of the total solid components. A small amount of CB nanoparticles was added in the anode, at 1 wt% of the total solid components.

To process the positive electrode, a total of 5-g solid components (ie, AM, PVDF, and CB) were manually mixed and ground in an agate mortar for 45 minutes. Then, the ground mixture was transferred to a 10-mL beaker, to which 2 mL of N-Methyl-2-pyrrolidone, or

TABLE 1 The cathode binders under investigation

Binder code	Polymer	Kynar ® grade	Molecular weight (by G.P.C)	HFP content (wt%)[26,27]	Melting point (°C)
PVDF (reference)	PVDF	711	180 000	0	165–172
TSB-1	PVDF-HFP	3120–50	-	10	161–168
TSB-2		2801–00	-	24	140–145
TSB-3		2501–20	500 000	32	117–125

NMP (Sigma-Aldrich, product no. 328634), was added for dissolving the PVDF binder. The solvent/power mixture was thoroughly mixed by an ultrasonic processor (Qsonica Q55) to form a slurry. To avoid overheating, the mixing was interrupted after every 1 minute, and the solution was cooled down in air for 2 minutes. This process was repeated 10 times. The anode slurry with PVDF binder was prepared following a similar process. For anodes with the CMC/SBR binder, the slurry processing followed the established MTI procedure.[16]

The wet cathode and anode slurries were cast on a 15-μm-thick aluminum substrate (MTI Corp., product code EQ-bcaf-15u-280) and a 9-μm-thick copper foil (MTI Corp., product code EQ-bccf-9u), respectively. The slurries were cast using a doctor blade (MTI Corp., product code EQ-Se-KTQ-100) and then dried at 80°C in a vacuum oven (VWR 1410) for 24 hours to completely remove the NMP solvent. For both anode and cathode, the initial slurry thickness was either 50 μm (for cycle life testing) or 200 μm (for nail penetration testing). After drying, the film thicknesses were reduced to 20–25 μm and 100–110 μm for thin and thick electrodes, respectively. The dried electrode films were sent through a hardened steel double roller to densify the electrode materials. Then, the film was cut into circular electrode disks of 14.3-mm diameter. In the final compressed state, a thin cathode disc contained about 8–10 mg AM, and a thick cathode disc contained about 30–35 mg AM.

Coin cell was assembled with a positive electrode and a negative electrode separated by a membrane separator. The cell case was CR2016 (Product No. T-2016 from Xiamen Tob). The AG mass in anode was slightly over 50% of the AM in the matching cathode, so that theoretical capacities of the 2 electrodes were compatible with each other. The membrane separator was a 25-μm-thick Celgard-2325 membrane. The active cell components were secured by a nickel foam, 14.3 mm in diameter and 1.6 mm in thickness (MTI Corp. EQ-bcnf-16 m). Finally, about 30 μL of electrolyte (BASF SelectiLyte-LP50) was added, and the assembled battery cell was at rest for 24 hours under ambient condition.

Nail penetration is a reliable method to trigger internal shorting of LIB CR2016 coin cell.[17] On the MTI BST8-3 Battery Analyzer, LIB cells with thicker electrodes were first conditioned with 1 charge-discharge cycle between 0 V and 4.3 V at 0.1 C, and then cycled between 4.2 V and 3 V at 0.5 C for 5 times, and finally charged to 4.6 V. The final capacity was approximately 5 mAh/cell. Immediately after charging, all the cells demonstrated a voltage drop to 4.50–4.52 V. After 10 minutes, the cells reached the stable voltage around 4.50–4.52 V, which was maintained for at least 3 hours. The cells were then pre-heated on a hot plate for 1 minute at 110°C. After heating, they were air-cooled to room temperature; the voltage maintained constant at 4.44–4.46 V for at least 10 minutes.

Nail penetration tests were performed on pre-cycled, fully charged, and preheated cells on a solid polyurethane (PU) holder as shown in Figure 1. The cell was attached onto the top surface of the holder by insulating tapes, topped off with a polyurethane foam layer for thermal insulation. A Palmgren bench vise was employed to drive a 1.58-mm-diameter stainless-steel nail through the center of the cell. The temperature of the cell was measured and recorded by a type-K gage-40 thermocouple (Omega TT-K-40-25), connected to a temperature logger (Omega OM-EL-USB-TC). The tip of the thermocouple was attached 3 mm away from the center of the cell.

Coin cells with thinner electrodes were used for cycle life testing with an MTI BST8-3 Battery Analyzer. The first cycle was performed between 3.0 V and 4.3 V at 0.1-C rate to establish the solid-electrolyte interface (SEI). The flowing cycles were performed between 3.0 V and 4.3 V at 1 C.

A closer analogue to commercial battery cells was produced by using the same cathode, anode, and electrolyte materials, but with a much larger cell size. The large pouch cells contained 10 layers of electrodes welded together, with the layer size of 76.2 × 76.2 mm. The reference cathode binder was PVDF, and the modified cathode binder was TSB-3. The anode binder was CMC/SBR. The large cells were charged at 0.7 A to 4.2 V, and discharged to 2.8 V at 0.7 A.

Differential scanning calorimetry (DSC) analysis was performed to characterize the cathode binders. For each sample, approximately 2 g of polymer was dissolved in 5-mL NMP, forming a gel. The gel was spread on a flat glass plate using a doctor blade. The casting thickness was ~1 mm. The material was then transferred to a vacuum oven for drying at 80°C for 24 hours, after which it conformed into a flexible film approximately 200 μm thick. The dried polymer film was cut into circular discs of 6.35-mm diameter, weighing approximately 10 mg

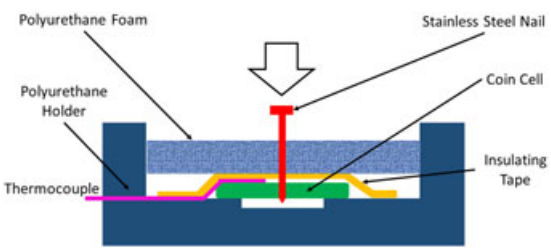

FIGURE 1 Schematic of the testing system of nail penetration [Colour figure can be viewed at wileyonlinelibrary.com]

each, and analyzed in a DSC 8000 machine (Perkin Elmer). The scanning temperature range was 40°C to 200°C, and the scanning rate was 10°C/minute.

3 | RESULTS

Figure 2 shows typical temperature increase profiles of coin cells in nail penetration tests. The temperature was measured 3 mm away from the center of the cell, simultaneously as the nail was driven through. Upon the nail penetration, in a reference cell, the temperature increases by ~2.75°C and ~2.45°C, for anodes based on CMC/SBR and PVDF, respectively. In a TSB-3 based cell, the temperature increases by ~1.75°C and ~1.85°C within 30 seconds, for anode binders of CMC/SBR and PVDF, respectively. As the HFP content decreases from TSB-1 to TSB-3, the temperature increase profile of the battery cell becomes lower.

Figure 3 shows the DSC results of the reference PVDF binder and the TSB, from 40°C to 200°C, at 10°C/minute. Table 2 summarizes their thermal properties. The DSC curve of the reference PVDF binder contains an endothermic peak at 166.74°C, associated with the melting that initiates at around 150°C and ends at 170°C; the peak is quite sharp and narrow. For every TSB, the DSC curve demonstrates a broad shoulder with a few secondary endothermic peaks before the main peak is reached. The melting points of TSB are also significantly lower than that of PVDF.

With the reference heat of fusion being set to 105 J/g for PVDF of 100% crystallinity,[18,19] it is calculated that the PVDF reference binder under investigation has a crystallinity of 42%. Theoretically, PVDF-HFP cannot achieve 100% crystallization and, thus, the exact reference heat of fusion is unavailable. Nevertheless, for the purpose of self-comparison, the crystallinities of PVDF-HEP are approximately assessed by using the same reference heat of fusion of 105 J/g. As shown in Table 2, it is evident that the higher the HFP content, the lower the heat of fusion and melting temperature would be; that is, the polymer tends to be more amorphous.

Scanning electron microscopy (SEM) analysis was performed on the reference and TSB-3 based cathodes at different stages of nail penetration. As shown in Figure 4A, B, no evident defects can be detected in the 2 electrodes after charging. The AM particles are densely packed in a similar way. After preheating, considerable swelling of TSB-3 is observed (Figure 4D). The binder-filled gaps among the AM particles become prominent (3–5 μm) in the TSB-3 based cathode (Figure 4D), while the reference PVDF binder is thermally stable up to 155°C and its

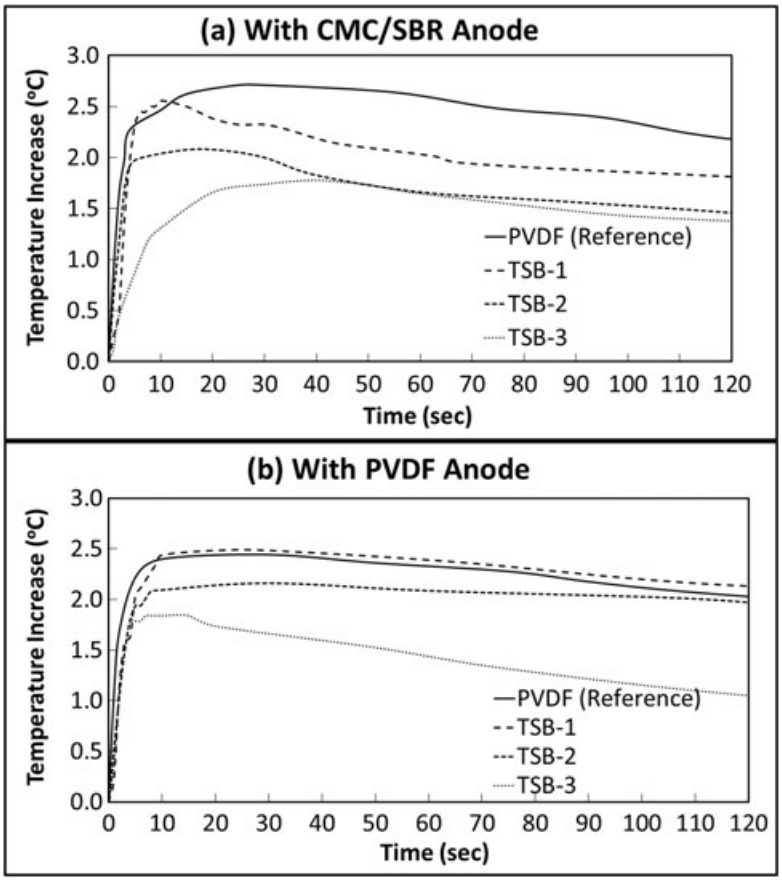

FIGURE 2 Typical temperature profiles in nail penetration tests of battery cells with anodes bound by (A) 4 wt% CMC/SBR (2:2) and (B) 6 wt% PVDF. The cathode binder is indicated by the legend

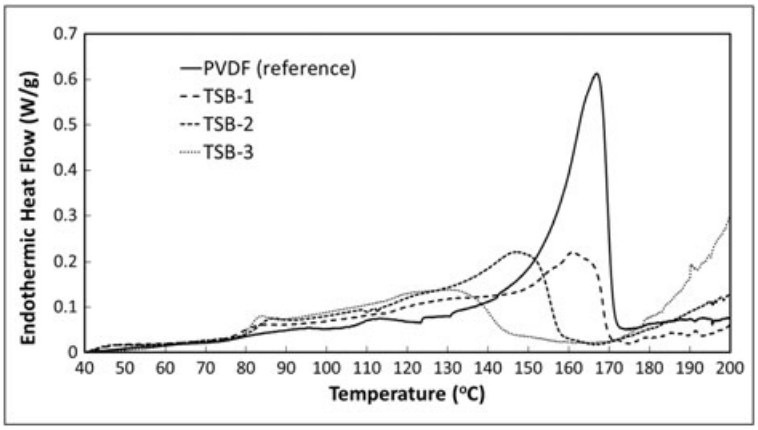

FIGURE 3 Typical DSC curves of solvent-processed cathode binders

TABLE 2 Thermal properties of cathode binders, obtained from the DSC analyses

	Melting point (°C)			
Binder code	**Onset**	**Peak**	**Heat of fusion, ΔH_f (J/g)**	**Crystallinity (%)**
PVDF (reference)	156	166	44	42
TSB-1	151	161	41	-
TSB-2	113	148	34	-
TSB-3	82	130	21	-

microstructure remains unchanged (Figure 4C). Figure 4F, which was taken far away from the nail, shows an ~2-μm gap between the separated AM particles in the TSB-3 electrode. In contrast, the bonding among AM particles and CB is intact in the reference electrode (Figure 4E).

Figure 5A,B shows the cycling performance of the reference and the TSB-3 cells. The discharge capacity is shown in percentage with respect to the capacity of the first 1-C rate discharge cycle, which is ~1.2 mAh for each cell. While the rest of the battery is the same, replacement of 4 wt% reference PVDF binder by 4 wt% TSB leads to a faster decay. When the PVDF is used as binder for anode, large fading of the TSB-based cell can be observed from the second cycle. When CMC/SBR is used as the anode binder, the TSB-based cell is quite stable for the first 50 cycles, after which the decay rate increases. Figure 5 shows the cycling performance of large pouch cells. The capacities at the first cycle were 2152 mAh and 1878 mAh for the reference and TSB-based cells, respectively (Figure 5C). It can be seen that the cycling performance of the TSB-based cell is much more stable than in a coin cell.

4 | DISCUSSION

Nail penetration reflects a simplified, intense condition of internal short circuit formation. In a large pouch cell, the local temperature increase (ΔT) near the nail penetration site often rapidly reaches 100°C to 200°C, which triggers thermal runaway.[20] For the small CR2016 battery cells in the current study, the amount of energy stored is limited, and the specific surface area is large. As a result, the peak temperature increase (ΔT_{max}) is less than 5°C. Therefore, it is critical to preheat the small coin cells to 110°C to simulate the effects of large temperature increase of a shorted large cell, eg, softening and swelling of TSB. The rapid heat generation, reflected by the steep initial slope, is a result of high-rate discharge.[21,22] As heat generation continues, it competes with the heat transfer,[21-23] and eventually ΔT enters a plateau region, followed by a gradual temperature decrease until the cell is completely discharged, ie, the stored electrochemical energy is dissipated. The temperature decrease section may be of interest for the investigation on the overall cell capacity and the discharge rate effects, yet the major goal of the TSB development is to slow down the heat generation rate in the initial stage.

For the TSB-based cells, the reduction in the heat generation rate should be related to the impedance increase of the TSB cathodes during preheating. At 110°C, the smallest crystalline areas in TSB are softened and become amorphous or melted. The polymer chains attract more electrolyte from adjacent fields, causing a sudden distortion of cathode morphology. The contact between CB and AM is loosened; the binding strength is much weakened. The internal impedance rises within

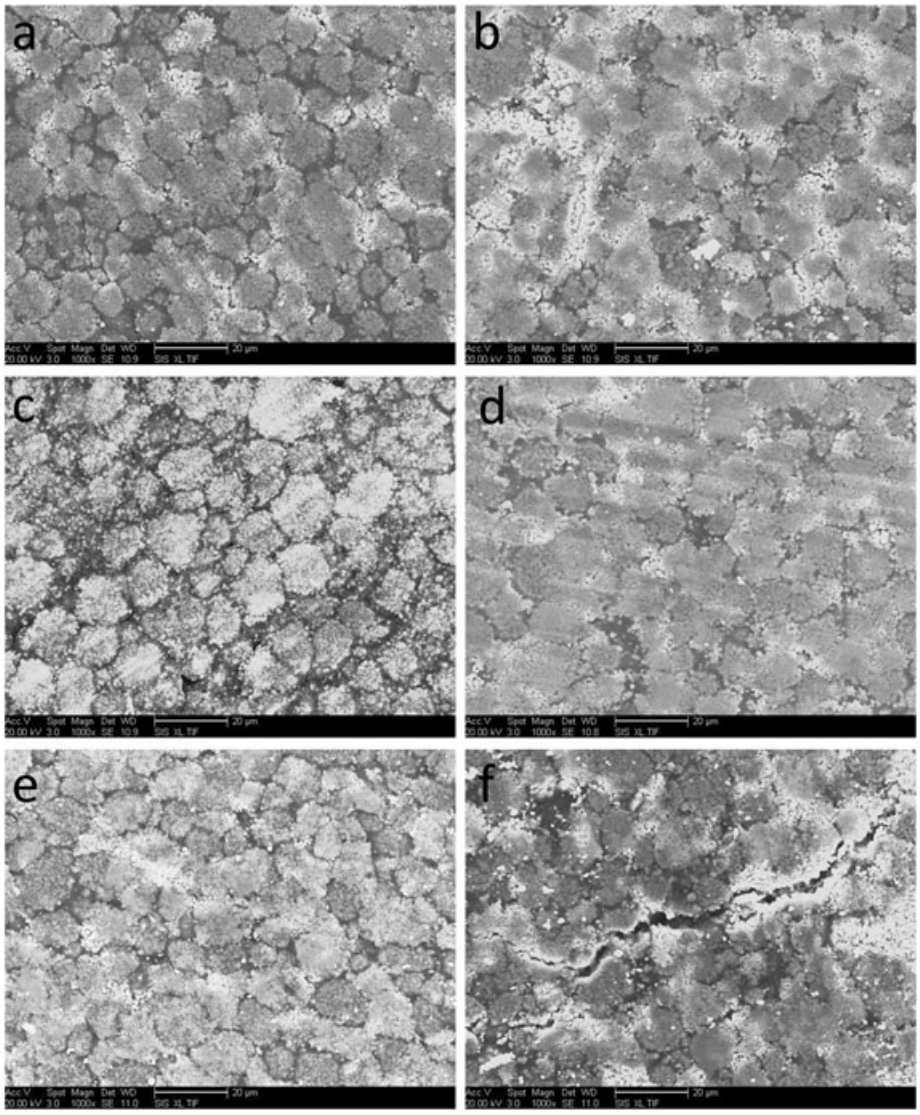

FIGURE 4 SEM images of reference positive electrodes (A, C, E) and TSB-based positive electrodes (B, D, F) at different stages: after cycling and charging (A,B), after preheating at 110°C (C, D), and after nail penetration, ~0.5 cm away from the nail (E, F)

the composite electrode layer and at the surface of current collector. Hence, the electron and ion transports are suppressed. TSB-3, with the highest content of HFP, attracts more electrolyte than TSB-1 and TSB-2, so that the internal impedance of the TSB-3 based cell increases more significantly, leading to the lower temperature increase.

For a cell with CMC/SBR anode, the peak temperature can be reached within 30 seconds after the nail penetrates through the cell. The initial slope of temperature profile is the lowest if the TSB-3 based cathode is used, suggesting that TSB has effectively disintegrated the active components of positive electrode. The peak temperature is reduced from 2.71°C in a reference cell to 1.74°C in a TSB-3 cell by ~36%. The CMC/SBR binder does not coat uniformly around the AG particles in anode, only creating bridges among these particles, which is more tolerant to the electrode morphology changes.

For cells with PVDF anodes, the peak temperature is reached within 10 seconds after the nail penetrates through. The initial slopes of the temperature profiles are almost the same for both reference cells and TSB-3 based cells. The peak temperature is reduced from 2.38°C in a reference cell to 1.84°C in a TSB-3 cell by ~23%. In contrast with the CMC/SBR binder, the PVDF binder uniformly coated the AG particles in anode. Such an anode is relatively stiff, and thus, the density of the compacted electrode layer is lower than that of CMC/SBR anode, resulting in a higher heat generation rate in the initial stage of nail penetration.

For large pouch cells, thermal runaway can happen within 1 minute after internal shorting takes place. In the current experiment, the peak temperature is reached within 10–30 seconds. The temperature increase is relatively small, mainly due to the Joule heating.[24] Although

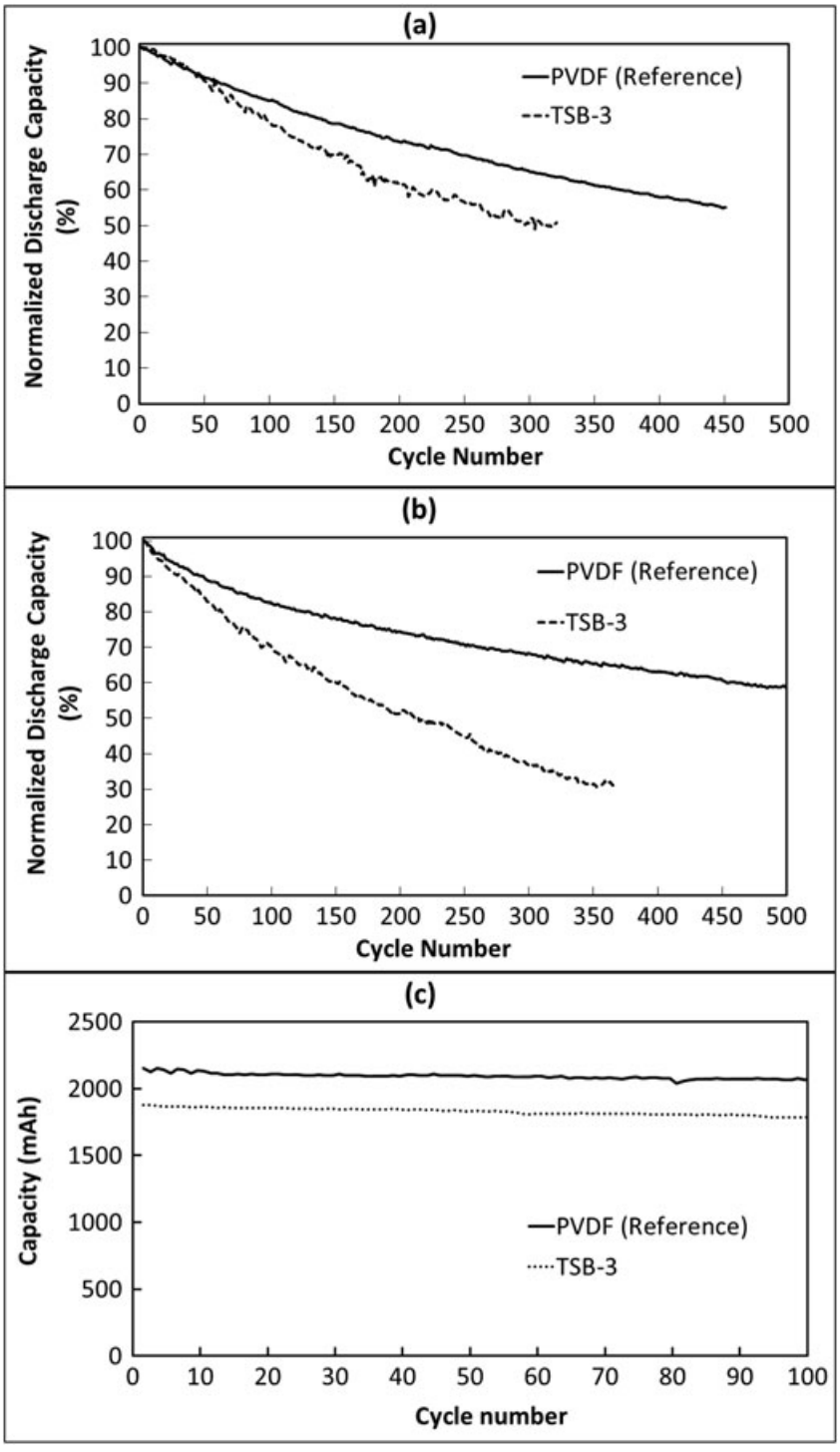

FIGURE 5 Cycling performance of coin cells, with the anodes based on (A) CMC/SBR binder and (B) PVDF binder. (C) Cycling performance of large pouch cells

no aggressive exothermic reactions are triggered, the testing data reflect the system behaviors at the early stage of heat accumulation, critical to the materials selection and battery cell design.

In the DSC curves (Figure 3), the shapes of the melting peaks are related to the variation in crystallinity. The reference PVDF is of a narrower distribution of the sizes of semi-crystalline phases, due to the refined molecular weight and the simpler molecular structure. The PVDF-HFP copolymers tend to have broad distributions of crystalline phase sizes, due to the broader variations in molecular weight and the HFP groups.[25] As a result, the number of smaller-sized semi-crystalline areas in TSB increases, which melt at lower temperatures. It is important to note the increasing slopes in the DSC curves after the major melting events have occurred. The slope becomes steeper with a higher content of HFP, which may be attributed to the higher volume expansion

associated with melting. The expansion of the polymer sample builds up an inner pressure, causing the deformation of the aluminum pan of the DSC machine.

The PVDF reference binder offers a high binding strength to the AM and CB components. However, the onset of melting of PVDF binder happens at a temperature much higher than the threshold point of thermal runaway (~110°C). For TSB, even though the main melting peak, related to the melting of the van de Waals bonds among the most abundant groups of the longest chains, occurs at a relatively high temperature, the broad shoulder shows up at ~80°C; ie, the binder works normally in the working temperature range of most LIB cells while begins to soften before thermal runaway accelerates.

Scanning electron microscopy images show no evident defects in both PVDF (reference) and TSB-3 based electrodes after precyling and charging (Figure 4A,B). Note that TSB-3 distributes more uniformly around the AM particles, probably because that TSB interacts with the NMP solvent more actively during slurry processing and it is also more deformable. The PVDF reference binder exhibits a higher resistance to solvent and calendaring. As a result, 1-μm to 2-μm large microscopic voids can be occasionally observed. The microvoids do not affect the electrochemical performance of the reference cathode, due to their small size and low number density, and also thanks to the sufficient binder strength.

After preheating, TSB-3 electrode exhibits significant swelling, with 3-μm to 5-μm binder-CB filled regions scattered across the electrode surface (Figure 4D). As temperature increases, the binder undergoes a phase transition from crystalline to amorphous and absorbs electrolyte from the surrounding regions. Recall that even though both reference and TSB cells show slight voltage drops after preheating, their voltages are stable for at least 10 minutes after air cooling, indicating that even though the microstructure of the TSB-3 electrode has been altered, its ability to host charges is not largely affected. However, the combined melting and swelling behaviors of the binder phase disintegrate the conducting network of CB additives and damage the electrical contact between the AM particles and the binder-CB phase. In addition, preheated TSB-3 becomes much weaker and is prone to separation upon the nail loading (Figure 4F). The damaged electrical contact and weakened bonding among the electrode components lead to a significant reduction in the temperature increase of the coin cell in nail penetration test.

The results of cycle life testing of coin cells (Figure 5A, B) suggested that replacing the conventional PVDF binder with TSB-3 binder leads to a faster capacity decay. Pouch cell testing shows a lower capacity for the TSB-3 based cell but a stable performance with relatively good capacity retention, suggesting that, with the large electrode thickness, TSB imposes less challenges as the cell size approaches the industrial level. However, after 110 cycles, the decay rate of the TSB-based cell tends to increase, probably due to the weak bonding strength between the electrode layers and the current collectors.

Clearly, the above research result does not facilitate a fully developed battery electrode binder technology. Issues related to the gradual swelling and loosening of TSB, the large amount of electrolyte absorbed in TSB, the relatively uniform distribution of TSB around AM particles, the thickness and density of SEI, the HFP content, as well as their influence on ion transport and reversibility must be further analyzed. Nevertheless, it is validated that TSB can significantly lower the heat generation rate of LIB cell immediately after it is damaged. It sheds much light on the study of safe and robust large-scale energy storage systems.

5 | CONCLUSIONS

In this study, heat generation of nail-penetrated LIB coin cells based on TSB was investigated. The TSB was PVDF-HFP. Upon nail penetration, with a high HFP content of 32 wt%, TSB can efficiently reduce the peak temperature of preheated cell by up to 36%; if the HFP content is relatively low (~24 wt%), this beneficial effect becomes secondary. The reduction in heat generation rate is related to the softening of TSB that begins at about 80°C. The binder softening not only weakens the bonding strength among AM particles, but also leads to more aggressive electrolyte absorption, both of which increase the internal impedance. The TSB, however, has a negative influence on the cycling performance of the LIB cells. Therefore, this technique may be most relevant to the applications where fire safety is highly prioritized and cell capacity may be slightly sacrificed, or the cell working condition is in favor of TSB, eg, when the working temperature is relatively low. We also tested CMC/SBR and PVDF as anode binders. They behave similarly, with the performance of the former being slightly better.

ACKNOWLEDGEMENT

This research is supported by the Advanced Research Projects Agency—Energy (ARPA-E) under Grant No. DE-AR0000396, for which we are grateful to Dr. Ping Liu, Dr. John Lemmon, Dr. Grigorii Soloveichik, Dr. Chris Atkinson, and Dr. Dawson Cagle.

REFERENCES

1. Liu C, Li F, Ma L-P, Cheng H-M. Advance materials for energy storage. *Advance Materials*, Volume. 2010;22 – Issue(8 (23 Feb):E38-E62.
2. Beguin F, Frackowiak E, Lu M. *Supercapacitors: Materials, Systems and Applications*. Wiley-VCH; 2013.
3. Torreglosa JP, García P, Fernández LM, FJurado F. Predictive control for the energy management of a fuel-cell–battery–supercapacitor tramway. *IEEE Transactions on Industrial Informatics*, Volume. 2014;10—No(1, (Feb):276-285.
4. Xu Q, Zhao TS. Fundamentals for flow batteries. *Prog Energy Combust Sci*. Aug 2015;49:40-58.
5. Park J, Park M, Nam G, Lee J, Cho J. Zinc-air batteries: all-solid-state cable-type flexible zinc-air battery. *Adv Mater* Volume. 27 – Issue(8 (25 Feb 2015)):1395
6. Liang X, Garsuch A, Nazar LF. Sulfur cathodes based on conductive MXene nanosheets for high-performance lithium-sulfur batteries. *Angew Chem Int Ed*, Volume. 54 – Issue(13 (Mar 2015)):3907-3911.
7. Xiong G, Meng C, Reifenberger RG, Irazoqui PP, Fisher TS. A review of graphene-based electrochemical microsupercapacitors. *Electroanalysis*. 2014;26(1):30-51.
8. Farmann A, Waag W, Marongiu A, Sauer DU. Critical review of on-board capacity estimation techniques for lithium-ion batteries in electric and hybrid electric vehicles. *J Power Sources*, Volume. 2015;281(1 May):114-130.
9. Li J, Daniel C, Wood D. Review—materials processing for lithium-ion batteries. *J Power Sources*, Volume. 2011;196, Issue(5, 1 March):2452-2460.
10. Ameduri B. From vinylidene fluoride (VDF) to the application of VDF-containing polymers and copolymers: recent development and future trends. *Chem Rev*. 2009;109:6632-6686.
11. Weicker P. A system approach to lithium-ion battery management. Artech House, 2013.
12. Balakrishnan PG, Ramesh R, Kumar TP. Review—safety mechanism in lithium ion batteries. *J Power Sources*. 2006;155:401-414.
13. Zhang SS. A review on the separators of liquid electrolyte Li-ion batteries. *J Power Sources*. 2007;164:351-364.
14. Chen Z, Chen Z, Hsu P-C, et al. Fast and reversible thermoresponsive polymer switching materials for safer batteries. *Nat Energy*, 11 Jan. 2016, Article No;15009
15. Feng XM, Ai XP, Yang HX. A positive temperature coefficient electrode for thermal cut-off mechanism for use in rechargeable lithium batteries. *Electrochem Commun*, Vol. 2004;6, Issue (10):1021-1024.
16. "A step by step recipe for preparing water-based electrode slurry (graphite anode)". MTI Corp.
17. Kim, G. H., Smith, K., Pesaran, A., "Lithium-ion battery safety study using multi-physics internal short-circuit model." The 5th International Symposium on Large Lithium-Ion Battery Technology and Application in Conjunction with AABC09, June 9–10, 2009, Long Beach, CA.
18. TA123, "Determination of polymer crystallinity by DSC", TA Instruments, New Castle, DE.
19. TN 48, "Polymer heats of fusion", TA Instruments, New Castle, DE.
20. Yoshio M, Brodd RJ, Kozawa A (Eds). *Lithium-Ion Batteries—Science and Technologies*. New York: Springer:32-61.
21. Terada N, Yanagi T, Arai S, et al. Development of lithium batteries for energy storage and EV applications. *J Power Sources*, Volume. 2001;100, Issues(1–2, November):80-92.
22. Pistoia G (Ed). *Lithium Ion Batteries: Advances and Applications*. Elsevier; 2014:419.
23. Sun Y-K, Myung S-T, Park B-C, Prakash J, Belharouak I, Amine K. High energy cathode material for long life and safe lithium batteries. *Nat Materials*, Volume. 2009;8, April:
24. Lin C-C, Wu H-C, Pan J-P, et al. Investigation on suppressed thermal runaway of Li-ion battery by hyper-branched polymer coated on cathode. *Electrochim Acta*. 2013;101:11-17.
25. TA276, "Determination of polymer crystal molecular weight distribution by DSC", TA Instruments, New Castle, DE.
26. Neese, B. P., "Investigations of structure-property relationships to enhance the multifunctional properties of PVDF-based polymers," 2009.
27. Terasawaa N, Onoa N, Hayakawac Y, et al. Effect of hexafluoropropylene on the performance of poly(vinylidene fluoride) polymer actuators based on single-walled carbon nanotube–ionic liquid gel. *Sens Actuators B*. 2011;160:161-167.

How to cite this article: Le AV, Wang M, Noelle DJ, et al. Using high-HFP-content cathode binder for mitigation of heat generation of lithium-ion battery. *Int J Energy Res*. 2017;1–9. https://doi.org/10.1002/er.3824